PCCP

PAPER

View Article Online
View Journal | View Issue

Cite this: *Phys. Chem. Chem. Phys.*, 2015, **17**, 24182

Unwilling U–U bonding in $U_2@C_{80}$: cage-driven metal–metal bonds in di-uranium fullerenes†

Cina Foroutan-Nejad,[ab] Jan Vícha,[bc] Radek Marek,[b] Michael Patzschke[d] and Michal Straka*[a]

Received 22nd July 2015,
Accepted 21st August 2015

DOI: 10.1039/c5cp04280a

www.rsc.org/pccp

Endohedral actinide fullerenes are rare and a little is known about their molecular properties. Here we characterize the $U_2@C_{80}$ system, which was recently detected experimentally by means of mass spectrometry (Akiyama *et al.*, *JACS*, 2001, 123, 181). Theoretical calculations predict a stable endohedral system, $^7U_2@C_{80}$, derived from the C_{80}:7 IPR fullerene cage, with six unpaired electrons. Bonding analysis reveals a double ferromagnetic (one-electron-two-center) U–U bond at an r_{U-U} distance of 3.9 Å. This bonding is realized mainly *via* U(5f) orbitals. The U–U interaction inside the cage is estimated to be about −18 kcal mol^{-1}. U–U bonding is further studied along the $U_2@C_n$ (n = 60, 70, 80, 84, 90) series and the U–U bonds are also identified in $U_2@C_{70}$ and $U_2@C_{84}$ systems at $r_{U-U} \sim 4$ Å. It is found that the character of U–U bonding depends on the U–U distance, which is dictated by the cage type. A concept of unwilling metal–metal bonding is suggested: uranium atoms are strongly bound to the cage and carry a positive charge. Pushing the U(5f) electron density into the U–U bonding region reduces electrostatic repulsion between enclosed atoms, thus forcing U–U bonds.

1 Introduction

Endohedral fullerenes and particularly endohedral metallofullerenes (EMF) have been extensively studied as promising materials for practical applications. Despite the great developments in EMF science[1–13] little is known of actinide endohedral fullerenes and their properties. Most of the experimentally reported actinide EMFs to date were only observed as signals in the time-of-flight mass spectra (TOF-MS), as for example $U@C_{2n}$ (n = 14–36) and some of the $U_2@C_{2n}$ (n = 25–30) systems.[14,15] Akiyama *et al.* reported a series of $An@C_{82}$ (An = U, Np, Am) as well as $An@C_{84}$ (An = Th, Pa) fullerenes,[16–19] and also $U_2@C_{80}$ that is of interest in this work. $U@C_{82}$ and $Th@C_{84}$ were prepared in larger amounts to be characterized by UV/vis/NIR spectroscopy.[16–19] The experimental formation of $U@C_{28}$ was studied recently.[20]

Actinide fullerenes have also attracted the attention of theoreticians. Mainly the $An@C_{28}$ compounds were studied.[21–26] The $An@C_{26}$ and $An@C_{40}$ series[27,28] and related compounds, such as $U@C_{36}$, $Pu@C_{24}$, and $U@C_{82}$, were investigated, too.[28–31] To the best of our knowledge, the experimentally observed $U_2@C_{80}$ molecule[17] has not been studied yet, and is the main concern of the present work.

The presence of two actinide atoms in a fullerene cage brings another interesting aspect that makes the endohedral actinide fullerenes attractive – the possibility of forming actinide–actinide bonds in the interior of a fullerene. Although numerous examples of metal–metal bonds for d-block elements have been documented in the transition-metal chemistry, actinide–actinide bonds are rare. The question of the existence of actinide–actinide bonding dates back to the early studies by Cotton *et al.*[32] and was revived by Gagliardi and Roos in 2005 in a study on U_2 system,[33] which is experimentally known,[34] followed by sequels on actinide diatomics,[35,36] and studies of various compounds with actinide–actinide bonds.[37–43]

Endohedral U–U bonding was suggested in 2007 by Wu and Lu[44] who studied theoretically the $U_2@C_{60}$ system, observed previously in TOF-MS experiments.[14,15] It was found, based on the MO framework, that the two U atoms confined in C_{60} form six one-electron-two-center (1e-2c, or ferromagnetic) metal–metal bonds at a calculated minimum U–U distance, r_{U-U} = 2.72 Å. Infante *et al.*[45] argued that the multiple U–U bonding in $U_2@C_{60}$ is, in fact, forced by the small interior of the cage. Hypothetical $U_2@C_{70}$ and $U_2@C_{84}$ fullerenes were calculated therein[45] but the

[a] *Institute of Organic Chemistry and Biochemistry, Academy of Sciences, Flemingovo nám. 2., CZ-16610, Prague, Czech Republic. E-mail: straka@uochb.cas.cz*
[b] *CEITEC - Central European Institute of Technology, Masaryk University, Kamenice 5/A4, CZ-62500 Brno, Czech Republic*
[c] *Centre of Polymer Systems, University Institute, Tomas Bata University in Zlin, Trida T. Bati, 5678, CZ-76001, Zlin, Czech Republic*
[d] *Helmholtz-Zentrum Dresden-Rossendorf, POB 510119, DE-01314, Dresden, Germany*

† Electronic supplementary information (ESI) available: Table S1 with *xyz* coordinates of $U_2@C_{80}$ lowest minimum and Fig. S1 and S2 with IR and Raman spectra of $U_2@C_{80}$ lowest minimum. Fig. S3 with Laplacian of spin density for $U_2@C_{80}$ and Fig. S4–S8 with frontier molecular orbitals for $^7U_2@C_n$ (n = 60, 70, 80, 84, 90) compounds. See DOI: 10.1039/c5cp04280a

U–U bonding in these systems was not investigated, possibly because of the calculated large U–U separation, $r_{U-U} \sim 3.9$ Å. Dai *et al.* predicted that in hypothetical $U_2@C_{90}$, the uranium atoms separate to $r_{U-U} \sim 6.1$ Å.[46]

A recent study has predicted the $UGd@C_{60}$ analogue of $U_2@C_{60}$ fullerene to have a large encapsulation energy and a high-spin 11-et ground state with a twofold one-electron U–Gd bond.[47] Studies of $U_2@C_{61}$ revealed that the exohedral carbon atom has a strong influence on the U–U distance and ground-state spin multiplicity. Such defects can be used for tuning the electronic properties of EMFs.[47,48]

Endohedral metal–metal bonding has been recently discussed in some experimentally known lanthanide and transition-metal fullerenes, for example, in $Y_2@C_{79}N$,[49] $Lu_2@C_{76}$,[50–52] and anionic $La_2@C_{80}$ fullerenes.[53] For more examples and references, see ref. 53 by Popov *et al.*, where the topic of endohedral metal–metal bonding is reviewed and studied in detail.

In this work we characterize fullerene $U_2@C_{80}$ by means of theoretical calculations. A stable endohedral system with large encapsulation energy for U_2 in the C_{80} cage is found. The energy and bonding analysis of $U_2@C_{80}$ provides evidence for metal–metal bonding interactions between the trapped uranium atoms. To further reveal the general trends in the endohedral U–U bonding we investigate a series of $U_2@C_n$ (n = 60, 70, 80, 84, 90) fullerenes and show newly the evidence for U–U bonding in hypothetical $U_2@C_{70}$ and $U_2@C_{84}$ cages as well as a correlation between the character of the U–U bonding and U–U distance inside a fullerene cage.

2 Methods

2.1 Molecular structure and properties

Following the previous experience,[45] calculations were done with the BP86 density functional using the def-SVP basis sets for C and U atoms[54,55] as implemented in the Turbomole 6.3.1 code. This basis set includes the effective core potential (SDD) for uranium atoms.[55] The structure search was done using Turbomole 6.3.1 and Gaussian 09 programs.[56,57] Natural population analysis (NPA) as implemented in the natural bond orbital[58,59] analysis implemented in Gaussian 09 was used. Molecular Orbitals were plotted using the Multifwn[60] and VMD software.[61]

The search for the geometry of the $U_2@C_{80}$ system was limited to the endohedral arrangement, $U_2@C_{80}$. This restriction is well justified by previous findings by Infante *et al.*[45] that the endohedral bonding of U_2 is strongly preferred to the exohedral arrangement in fullerenes C_{60}, C_{70}, and C_{84}. In search for the lowest $U_2@C_{80}$ minimum, local minima were searched by placing the U_2 unit (at r_{U-U} = 2.5 Å) in the center of the C_{80} cage along three different orientations (x, y, or z axis). All seven IPR C_{80} cages were checked by this procedure. The systems were minimized maintaining the septet electron state[44,45] without symmetry constraints. The septet ground state was confirmed by calculating triplet, quintet, and nonet (all geometry optimized). The quality of the unrestricted Kohn–Sham wavefunction was confirmed by negligible spin-contamination, <0.1. The minima were checked by frequency analysis.

The empty C_{80}:7 cage has topological I_h symmetry which is a saddle point due to orbital degeneracy. The empty cage undergoes the Jahn–Teller distortion to a D_2 structure.[62] For the encapsulation energy calculations we used the C_{80}:7 (I_h) geometry as a starting point and minimized it under D_2-symmetry constraints in the singlet ground state.

2.2 QTAIM analysis

The topological properties of critical points within the context of the Quantum Theory of Atoms in Molecules (QTAIM)[63] have been employed many times for analyzing the bonding properties in various materials[64] including fullerenes, see, *e.g.* ref. 53 and 65–67.

However, as some of us have shown recently,[68] the presence or absence of line critical points (LCP) in a single geometry neither confirm nor invalidate the presence of a chemical bond. In this work, we rely on the profiles of the derivatives of the electron density and a unique quantitative measure of the covalency within the context of QTAIM, delocalization index, $\delta(A \leftrightarrow B)$ or DI.[68]

Of the topological profiles, the Laplacian of the electron density, $\nabla^2\rho(r)$, has been conventionally used to identify the electron density concentration (EDC) between atoms that are believed to be linked to covalency.[63] Besides $\nabla^2\rho(r)$, energy density, $H(r)$, has been proposed to be an efficient tool for distinguishing covalent and polar covalent chemical bonds.[69] Energy density at any point in space is defined as $H(r) = V(r) + G(r)$, where $V(r)$ and $G(r)$ are potential and gradient kinetic energy densities. $V(r)$ is always negative at any point in space but $G(r)$ is always positive; a negative $H(r)$ value denotes the dominance of potential energy at a point, which has been interpreted in favour of covalency.

The DI defines the number of electrons that are shared between any pair of atoms,

$$\delta(A \leftrightarrow B) = -2[\langle n_A n_B\rangle - \langle n_A\rangle\langle n_B\rangle], \quad (1)$$

where $\langle n_A n_B\rangle$, $\langle n_A\rangle$, $\langle n_B\rangle$ are the localization index or in other word, the minimum electron populations of the atomic pair and single atoms, respectively.

The DI was suggested as a direct measure of electron exchange between atomic basins of two atoms A and B. Recent studies demonstrate that $\delta(A \leftrightarrow B)$ quantitatively reflects the magnitude of the exchange–correlation energy component for an atomic pair A–B.[70,71] The magnitude of DI is close to unity for a typical single homonuclear (sigma) bond, *e.g.* a carbon–carbon bond in ethane.[72] The magnitude of DI for a homonuclear bond reflects the bond order, *e.g.*, it is close to 2, 3, and 4 for double, triple, and quadruple homonuclear bond, respectively. On the contrary, DI of a polar-covalent bond is smaller than the expected value based on the MO picture, which is consistent with chemical intuition for the formation of a polar covalent bond. Nevertheless, it is highly recommended to compare the DI of any system with an external reference to characterize the bond order of a system. Here, we chose U_2 as

our external reference for assessing the bond order between uranium atoms in the fullerene systems. Scalar-relativistic computations predicted that U_2 has a quintuple bond.[33] Studying the $\delta(U \leftrightarrow U)$ of U_2 molecule, optimized at the same level of theory as $U_2@C_{80}$, demonstrates that the DI can recover the bond order of this system in a good agreement with previous studies; $\delta(U \leftrightarrow U) = 5.08$.

The wavefunction for the analysis of the electron density of the minimum structure was obtained at the BP86/SVP/SDD computational level (*cf.* above) by Gaussian 09.[56] The electron density was analyzed within the context of the QTAIM[63] by AIMAll suite of programs.[73] For properly treating the uranium atoms in QTAIM analysis, auxiliary basis functions were added to the wavefunction of the molecule.[73]

3 Results and discussion

3.1 U_2C_{80} is a stable endohedral $U_2@C_{80}$:7 system with a septet ground state. U–U interactions inside the cage are attractive

Endohedral compounds of the $M_2@C_{80}$ formula, so far experimentally observed, are either $M_2^{IV}C_2@C_{78}$ systems, such as $Ti_2C_2@C_{78}$, or $M_2^{III}@C_{80}$ systems, such as $Ce_2^{III}@C_{80}$ fullerenes.[4,74–76] Because the ionic radii of U^{III} and Ce^{III} are almost identical, 1.16 Å and 1.15 Å, while those of Ti^{IV} and U^{IV} are substantially different, 0.745 Å and 1.03 Å, ref. 77, it can be assumed that an $U_2^{III}@C_{80}$ system would be formed rather than an $U_2^{IV}C_2@C_{78}$ system.

The lowest energy minimum structures for each of the seven possible IPR (isolated pentagon rule)[78] C_{80} cages with enclosed U_2, assuming the septet ground state,[44–46] *i.e.*, six unpaired electrons, are listed in Table 1. The lowest energy minimum derives from the C_{80}:7 cage whereas the optimized minima based on other IPR cages are *ca.* 10–40 kcal mol^{-1} less stable. Indeed, the $U_2C_2@C_{78}$ isomer was calculated *ca.* 20 kcal mol^{-1} higher in energy than the most stable $U_2@C_{80}$ isomer, Table 1.

Table 1 Calculated relative energies[a], ΔE, and U–U distances[b], r_{U-U}, for the IPR-based $U_2@C_{80}$ isomers and $U_2C_2@C_{78}$:5 system[c]

System	ΔE [kcal mol^{-1}]	r_{U-U} [Å]
$^7U_2@C_{80}$:1	42.5	5.117
$^7U_2@C_{80}$:2	35.0	5.030
$^7U_2@C_{80}$:3	21.2	3.728
$^7U_2@C_{80}$:4	22.8	4.198
$^7U_2@C_{80}$:5	10.5	3.871
$^7U_2@C_{80}$:6	11.8	3.901
$^3U_2@C_{80}$:7	22.9	3.965
$^5U_2@C_{80}$:7	18.0	3.903
$^7U_2@C_{80}$:7	**0.0**	**3.894**
$^9U_2@C_{80}$:7	13.4	3.872
$^3U_2C_2@C_{78}$:5	20.1	4.256
$^5U_2C_2@C_{78}$:5	29.8	4.326
$^7U_2C_2@C_{78}$:5	42.1	4.325

[a] Relative electronic energies wrt the ground state $^7U_2@C_{80}$:7 calculated at the BP86/SVP/SDD level. [b] The closest U–C_{cage} distances are 2.35–2.50 Å. The U–C_{endo} distances in $U_2C_2@C_{78}$ are between 2.20 and 2.30 Å. [c] Singlet $^1U_2@C_{80}$:7 could not be converged.

The optimized structure of $^7U_2@C_{80}$:7 is shown in Fig. 1. The molecule has C_i symmetry with the two uranium atoms located nearby a D_3 axis of theC_{80}:7 cage. Analogous $^3Ce_2^{III}@C_{80}$:7 has a D_{3d} minimum structure with the cerium atoms and the two closest carbons located on a D_3 axis.[75] (It is a dynamical system, though.[76]) Attempted optimization of $^7U_2@C_{80}$:7 within D_{3d} constraints did not converge to a stationary point. At the present level of theory a C_{2h}-symmetric stationary point (one imaginary frequency) could be found about 1 kcal mol^{-1} above the C_i minimum. With such a small difference, it cannot be excluded that the C_{2h} stationary point becomes the lowest minimum if different computational levels are used.

The U–U distance in the $^7U_2@C_{80}$:7 minimum structure of 3.89 Å is rather long as compared to that predicted for $U_2@C_{60}$ (~2.72–2.74 Å),[44–46] or in bare U_2 and U_2^{2+} (~2.43 and ~2.30 Å).[33,35,45] It is also longer than twice the empirical single-bond radius of uranium (2 × 1.7 Å = 3.4 Å),[79] which suggests the U–U bond order lower than one. However, see below.

The closest U–C bond lengths in $^7U_2@C_{80}$:7 minimum are 2.40, 2.48, and 2.51 Å, comparable to those found in the strongly bound $U@C_{28}^{2+}$, where the r_{U-C} closest contacts are within 2.44–2.51 Å.[25] In fact, the cage is significantly stretched along the U–U axis in $^7U_2@C_{80}$:7. The end-to-end distances between the carbon atoms connecting three hexagons on opposite sides of the cage (Fig. 1) vary from 8.16 to 8.33 Å in the empty C_{80}:7, and elongate to 8.68 Å along the U–U axis and to 8.20 Å in the direction perpendicular to the U–U axis in the $^7U_2@C_{80}$:7 minimum structure.

The septet ground state of $U_2@C_{80}$:7 with six unpaired electrons was confirmed by calculating the geometry-optimized nonet, quintet, and triplet, which lay 13, 18, and 23 kcal mol^{-1} above the ground state septet, Table 1. Note that the previously studied di-uranium fullerenes, $U_2@C_{60}$, $U_2@C_{70}$, $U_2@C_{84}$, and $U_2@C_{90}$, were predicted to be septet in their ground state.[44–46] These findings point to a general pattern in the electronic structure of $U_2@C_{2n}$ fullerenes. For the future experimental reference, the predicted structure, IR, and Raman spectra of the $^7U_2@C_{80}$:7 lowest minimum structure are given in Table S1 and Fig. S1 and S2 in the ESI.†

The encapsulation energy, ΔE, for the $^7U_2(g) + C_{80}(g) = {}^7U_2@C_{80}$:7 reaction was calculated to be −252.7 kcal mol^{-1} at the BP86/SVP/SDD level. The reaction enthalpy, approximated by the sum of the electronic and zero-point energy was predicted slightly lower, $\Delta H = -248.6$ kcal mol^{-1}. These results are consistent with the previous findings for $U_2@C_{60}$, $U_2@C_{70}$, and $U_2@C_{84}$ where the encapsulation energy was ranging from −160 to −210 kcal mol^{-1}.[44,45] For a further comparison, we calculated encapsulation energies for the experimentally known analogous $La_2@C_{80}$ and $Ce_2@C_{80}$ complexes. The calculated ΔE for the $M_2(g) + C_{80}(g) = M_2@C_{80}(g)$ reaction[80,81] is predicted to amount to −255 and −257 kcal mol^{-1} for M = La, Ce at the BP86/SVP/SDD level.

Interaction between the enclosed uranium atoms in $U_2@C_{80}$ can be actually estimated from a hypothetical isodesmic reaction $2U_1@C_{80} = U_2C_{80} + C_{80}$. Thanks to the symmetry of the system, the left side of the reaction corresponds to twice the

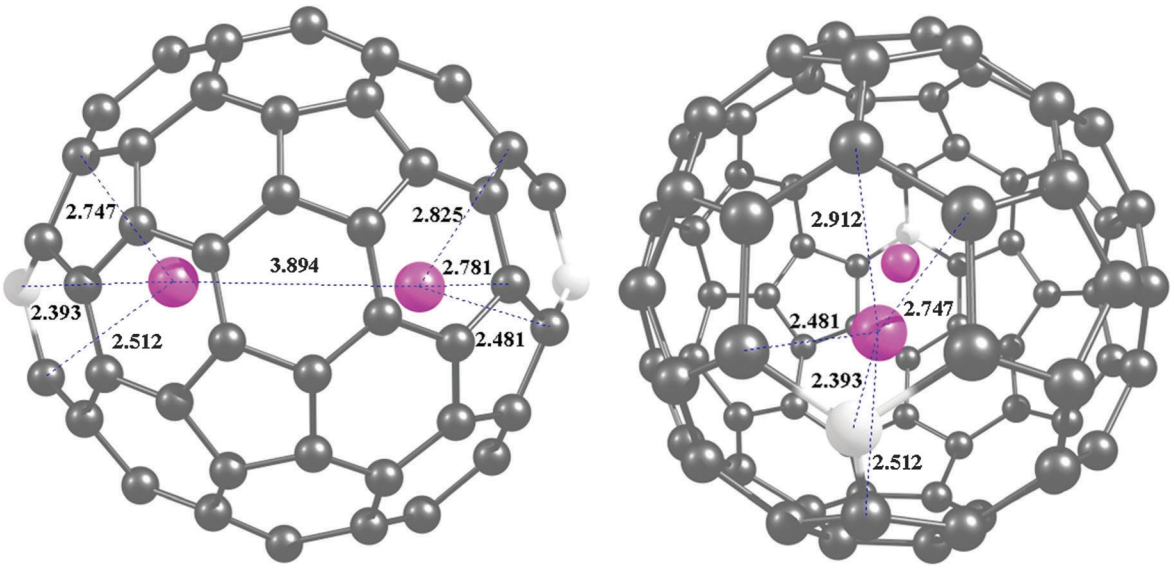

Fig. 1 The $^{7}U_2@C_{80}$:7 minimum structure calculated at the BP86/SVP/SDD level.

U–cage interaction and the right side has twice the U–cage plus the U–U interaction in it. The $\Delta E = -17.7$ kcal mol^{-1} is in favour of products and gives a thermodynamical evidence for endohedral U–U bonding interactions in $U_2@C_{80}$. This evidence is further supported by the bonding analysis given below.

Apparently, the encapsulation energy for $U_2@C_{80}$ of ~ -250 kcal mol^{-1} is substantially larger than the U–U interaction estimated above, or than the dissociation energy of U_2, which was calculated to be -70.1 kcal mol^{-1} at the BP86/SVP/SDD level or -33.6 kcal mol^{-1} at the CASPT2 level at corresponding equilibrium distance ($r_{U-U} \sim 2.7$ Å).[44,45] One may thus expect that the weaker U–U bonding will be strongly affected by the size/type of the cage keeping each uranium atom at a position dictated by the stronger U–C bonding, see Section 3.4.

3.2 MO analysis reveals endohedral U–U bonding orbitals in $U_2@C_{80}$

It is well known that in $M_2@C_{80}$:7 systems, the C_{80}:7 cage formally accepts six electrons from the confined metal atoms.[4,65] At the ionic limit, this leads to a C_{80}^{6-} cage interacting with two positively charged M^{3+} ions. However, the electrons are not fully localized on the cage but they are partly shared between the cage and the enclosed cluster.[4,65] The bonding situation in $^{7}U_2@C_{80}$:7 is akin to previously studied $M_2@C_{80}$ compounds. The level of electron transfer is seen on the calculated NPA charge on each uranium atom, $q_U = +0.82$ and on the natural electron configuration (U:7s$^{0.21}$5f$^{3.54}$6d$^{0.98}$) of enclosed atoms in comparison with the ground state configuration of neutral uranium atoms (U:7s^{2}5f^{3}6d^1). The six unpaired electrons in $^{7}U_2@C_{80}$:7 are mainly in the U(5f) shell, and are, in fact, strongly localized between the encapsulated uranium atoms as seen from NPA analysis (details not shown) and the frontier orbitals in Fig. 2.

A closer look at the frontier singly-occupied molecular orbitals (SOMO) in Fig. 2 reveals a bonding situation between the enclosed uranium atoms. The SOMO and SOMO−1 orbitals have U–U antibonding character whereas the SOMO−2 through SOMO−5 have U–U bonding character. This situation can be interpreted as two (four bonding minus two antibonding) 1e-2c bonds, in other words a double ferromagnetic bond between the encapsulated uranium atoms. This bond is clearly U(5f)-based. The localization of the unpaired electrons between the uranium atoms is identified also by the calculated spin density in Fig. 3. The localization of the spin density on uranium atoms and its presence on some of the cage carbon atoms may allow for the future experimental identification of the $U_2@C_{80}$ system by ESR[49,82] or paramagnetic ^{13}C NMR spectroscopy.[83–85]

3.3 QTAIM analysis gives evidence for a single U–U bond in $U_2@C_{80}$:7

The bonding between the encapsulated U–U atoms in $U_2@C_{80}$ is further studied by the QTAIM analysis (for details on QTAIM, see Methods section). In this work, rather than on the presence or absence of line critical points we rely on the profiles of the derivatives of the electron density and a unique quantitative measure of the covalency within the context of QTAIM, the delocalization index, $\delta(A \leftrightarrow B)$.[68]

Inspecting the Laplacian of the alpha-electron density reveals electron density concentration (EDC) between the uranium atoms, Fig. 4b, a.k.a. U–U bonding interaction. Interestingly, the EDC between the U atoms is not recognizable in the Laplacian of the total electron density, Fig. 4a, since the overall electron density masks the alpha-EDC between the uranium atoms, shown in Fig. 4b. An interesting picture emerges from the Laplacian of the spin density, Fig. 4c, which highlights the regions of spin-density concentration. A profile of f-orbitals and an EDC between two uranium atoms resulting from the f-orbital overlap is rather evident in Fig. 4c. For 3D representations of Fig. 4c, see Fig. S3 (ESI†).

In the contour map of energy density, $H(r)$, Fig. 4d, the C–C, U–C and U–U bonds fall in the negative energy density regions,

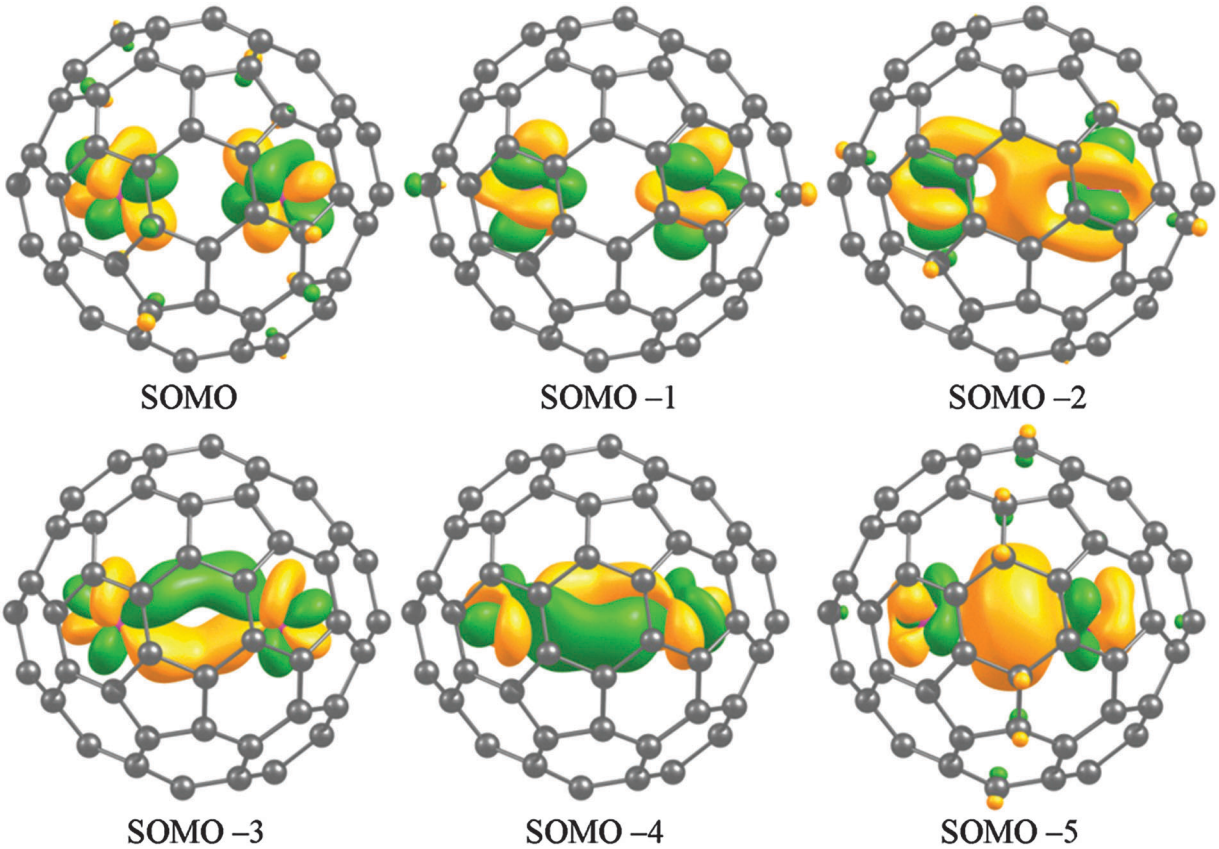

Fig. 2 The six highest singly-occupied molecular orbitals (SOMOs) of the $^{7}U_2$@C_{80}:7 system.

denoting a total stabilization arising from the covalent-type interactions, *i.e.* electron sharing among the cage carbon atoms, the carbon and the uranium atoms, and between the two uranium atoms.

The delocalization index, DI, for the U–U bond, δ(U ↔ U) was calculated to be 1.01 in $^{7}U_2$@C_{80}:7. Comparing this value with that for U_2 with a quintuple bond calculated at the same level of theory, δ(U ↔ U) = 5.08, suggests that U–U bonding in the U_2@C_{80}:7 molecule corresponds to a single U–U bond. This is consistent with the MO picture of two 1e-2c U–U bonds in Fig. 2 above. Notably, calculated δ(M ↔ M) indices for Sc–Sc, Y–Y, Lu–Lu, or La–La interactions in similar dimetallofullerenes were found comparably lower than one,[53] within 0.25–0.65, albeit obtained at different levels of theory. The largest value found was δ(Lu ↔ Lu) of 0.65 in Lu_2@C_{82} at r_{Lu-Lu} = 3.476 Å. Details can be found in ref. 53.

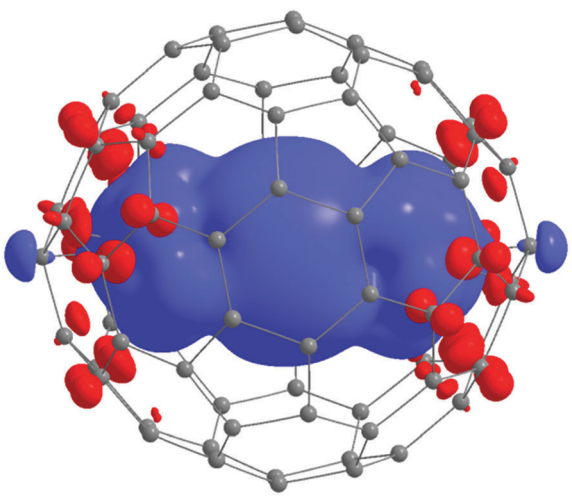

Fig. 3 The calculated ground-state spin density for the U_2@C_{80}:7 system.

The energetically higher multiplets of U_2@C_{80}:7 (Table 1) give similar DI as that for the septet, δ(U ↔ U) = 1.02 for the triplet and δ(U ↔ U) = 1.37 for the quintet state. Nonet could not be analyzed. The larger DI value for the quintet state is given by the fact that the corresponding electron moves from an U–U alpha antibonding to an U–U beta bonding orbital, while r_{U-U} = 3.90 Å remains similar to that for the septet ground state, where r_{U-U} = 3.89 Å, Table 1.

The magnitude of δ(U ↔ C) for single pair of atoms was found in the range of 0.12 to 0.36 for carbon atoms, which are within the distance of 2.98–2.39 Å from the uranium atoms. These values are within the range of the typical metal–carbon delocalization indices.[72]

We have thus seen strong theoretical evidence for U–U bonding in the $^{7}U_2$@C_{80}:7 system, *via* the attractive U–U potential inside the cage, the presence of a double ferromagnetic bond, or the QTAIM delocalization index for U–U of 1.01.

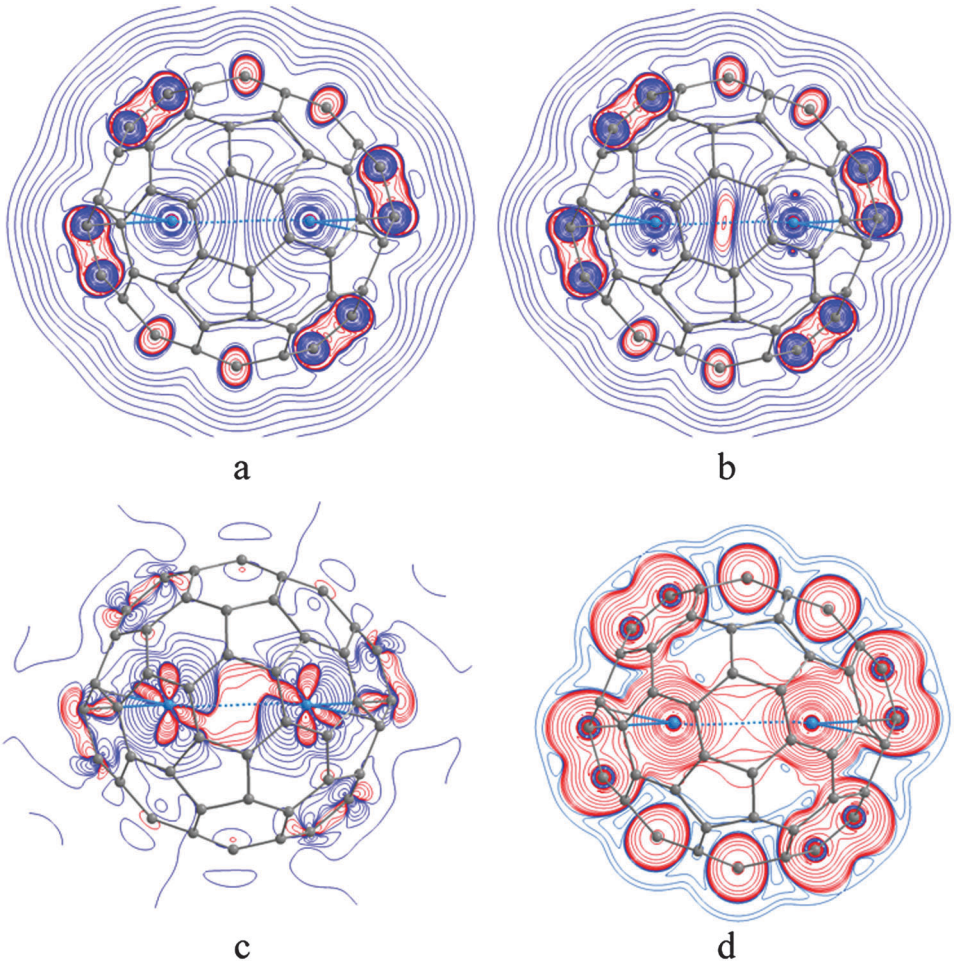

Fig. 4 Contour maps of (a) Laplacian of electron density, (b) Laplacian of alpha-electron density, (c) Laplacian of spin density, and (d) energy density in the $^{7}U_2@C_{80}$:7 system; negative functions in all plots, implying electron concentration/sharing are presented by red lines.

Notably, this U–U bonding is actually observed at relatively large r_{U-U} = 3.89 Å, which is beyond the sum of empirical single-bond radii of uranium of 2 × 1.7 = 3.4 Å.[79] The endohedral metal–metal bonding at large M–M separations was recently noted for di-lanthanofullerene anions $La_2@C_n^{q-}$, where r_{La-La} as large as 3.7–5.2 Å gave δ(La ↔ La) = ∼0.3, ref. 53 Hence, we decided to investigate a series of previously studied di-uranofullerenes to estimate how far can the U–U bonding reach and what are the cage-driving capabilities of fullerenes for U–U bonding.

3.4 The U–U bonding along the $U_2@C_n$ series reaches beyond $U_2@C_{80}$ and is determined by the cage type

In the following we shortly analyze the U–U bonding interactions and trends in the series of diuranium fullerenes, $U_2@C_n$ (n = 60, 70, 80, 84, 90).[14,17,44–46] The selection of C_{70}–C_{90} cages was motivated solely on the basis of previous studies[45,46] to illustrate the metal–metal bonding *vs.* the size of the cage; lower-energy isomers may exist but were not searched for. Optimized structures of $U_2@C_n$ are shown in Fig. 5. Selected properties, calculated at the BP86/SVP/SDD level, are summarized in Table 2. We note that only $U_2@C_{60}$ and $U_2@C_{80}$ of the species in Table 2 have been observed experimentally so far.[14,17]

$^{7}U_2@C_{80}$ has the largest U_2 encapsulation energy (−252.7 kcal mol^{-1}) among the studied systems. Generally, the encapsulation energy of diuranium EMFs lies in the range of −150 to −250 kcal mol^{-1}, Table 2.

The U–U distance and the degree of U–U bonding, expressed by the δ(U ↔ U) along the series in Table 2, in fact correlate with the (relative) size of the fullerene cage. No correlation with the encapsulation energies is observed. As noted for $U_2@C_{80}$, the encapsulation energy along the $U_2@C_n$ series is substantially larger (150–250 kcal mol^{-1}) than the energy of U–U binding in bare U_2 (70.1 kcal mol^{-1} at the BP86/SVP/SDD level).[45] The U–U interaction inside the cage is thus to a large extent dictated by the U–cage bonding. This argument is further supported by rather constant r_{U-C} contact distances along the series, whereas r_{U-U} is changing substantially, as seen in Table 2.

Following the U–U distance and δ(U ↔ U) along the series, we confirm the argument of Infante *et al.*[45] that multiple U–U bonding in $U_2@C_{60}$ is forced by the short U–U distance in the small cage interior. In a large enough cage, like C_{90}, the uranium atoms separate and practically do not interact with each other.[46] This is confirmed by negligible δ(U ↔ U) = 0.1 in $^{7}U_2@C_{90}$. The present results show newly the evidence for the

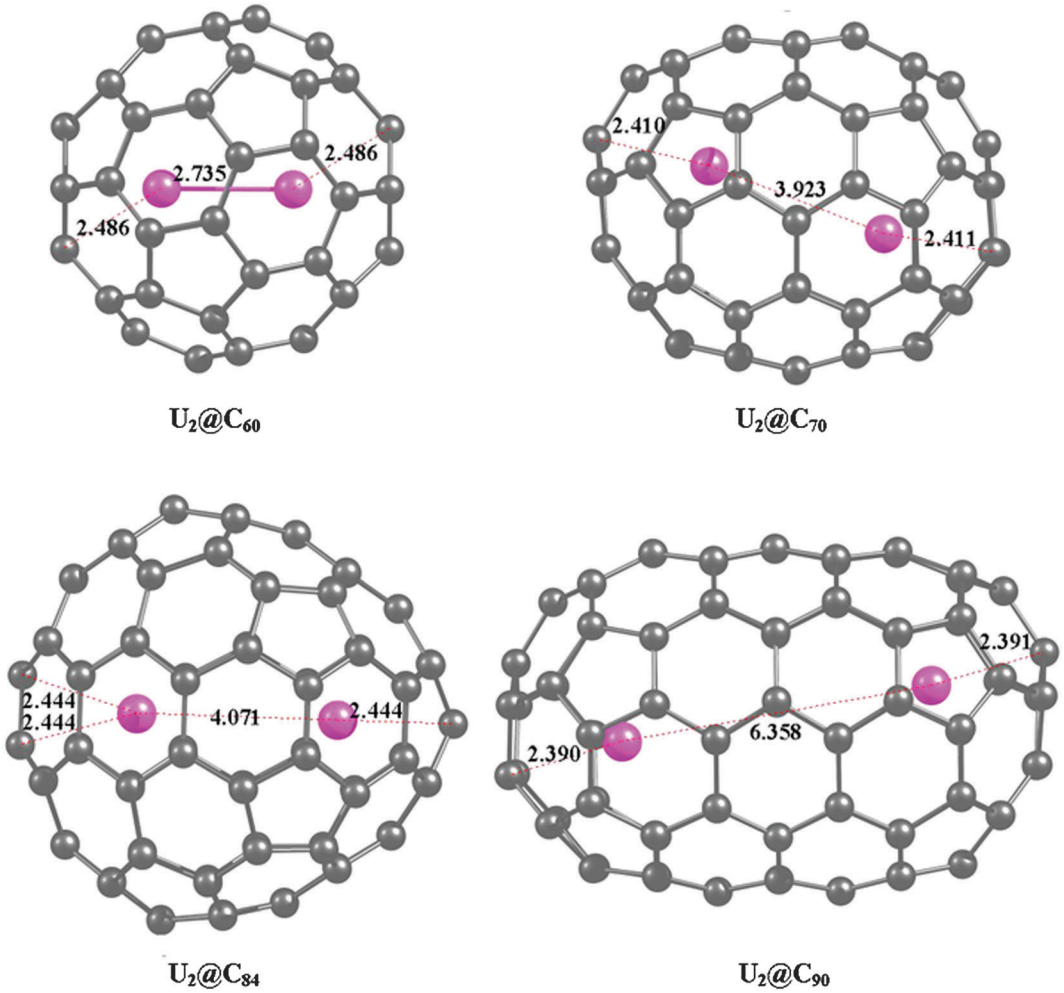

Fig. 5 Optimized structures of $U_2@C_{60}$, $U_2@C_{70}$, $U_2@C_{84}$, and $U_2@C_{90}$. The U–U and closest U–C interactions are shown by dotted lines with the corresponding interatomic distances.

Table 2 The U–U and U–C distances, the encapsulation energies for the $^7U_2 + C_n \rightarrow {}^7U_2@C_n$ reaction, calculated NPA charge on U atoms, delocalization indices for U–C and U–U bonding, and NPA populations on uranium atoms in the $^7U_2@C_n$ (n = 60, 70, 80, 84, 90) EMFs. Calculated at the BP86/SVP/SDD level

System	r_{U-U} [Å]	r_{U-C} [Å]	ΔE [kcal mol^{-1}]	q_U	δ(U ↔ U) [au]	$\sum\delta$(U ↔ C) [au]	NPA on U
$^7U_2@C_{60}$	2.735	2.48–2.49	−200.7	0.07	2.1	4.5	$7s^{0.13}5f^{4.18}6d^{1.16}$
$^7U_2@C_{70}$	3.923	2.40–2.65	−189.1	0.41	0.7	4.9	$7s^{0.21}5f^{3.76}6d^{1.03}$
$^7U_2@C_{80}$	3.894	2.40–2.54	−252.7	0.82	1.0	4.1	$7s^{0.21}5f^{3.54}6d^{0.98}$
$^7U_2@C_{84}$	4.071	2.44–2.67	−152.2	0.78	0.7	4.4	$7s^{0.24}5f^{3.62}6d^{0.92}$
$^7U_2@C_{90}$	6.358	2.39–2.64	−183.0	0.74	0.1	4.9	$7s^{0.08}5f^{3.73}6d^{0.88}$

U–U bonding also in cages of intermediate size, $U_2@C_{70}$ through $U_2@C_{84}$, with $r_{U-U} \sim$ 3.9–4.0 Å, as indicated by the QTAIM delocalization index, δ(U ↔ U) = 0.7–1.0 in Table 2.

The QTAIM analysis shows some general features along the studied series, as is evident from Fig. 6. The EDC, corresponding to the U–U interaction, is absent in the Laplacian of electron densities of $U_2@C_{60}$ and $U_2@C_{70}$ (Fig. 6, panels 1a and 2a) but it appears for that of $U_2@C_{84}$ (Fig. 6, panel 3a). The EDC is also absent in the Laplacian of alpha-ED of $U_2@C_{60}$ (Fig. 6, panel 1b) but appears for the $U_2@C_{70}$ through $U_2@C_{84}$ (Fig. 4b and Fig. 6, panels 2b and 3b). This is due to the masking effect of the electron density of carbon atoms and also the masking of the alpha-ED by beta-ED in the total ED of smaller cages. In all compounds, the Laplacian of the spin density unveils the pattern of f-orbitals involved in accommodating the unpaired 5f-electrons (Fig. 6, panels 1c–4c). The energy-density profiles (Fig. 6, panels 1d–4d) delineate covalently bonded atoms. Notably, the level of U–U interaction can be easily identified qualitatively from the energy density profiles. The strongest effect is seen in $U_2@C_{60}$ and $U_2@C_{80}$, weaker in $U_2@C_{70}$ and $U_2@C_{84}$, and the profile of $U_2@C_{90}$ points to the absence of U–U interaction, see Fig. 6, panels 1d–4d, and Fig. 4d.

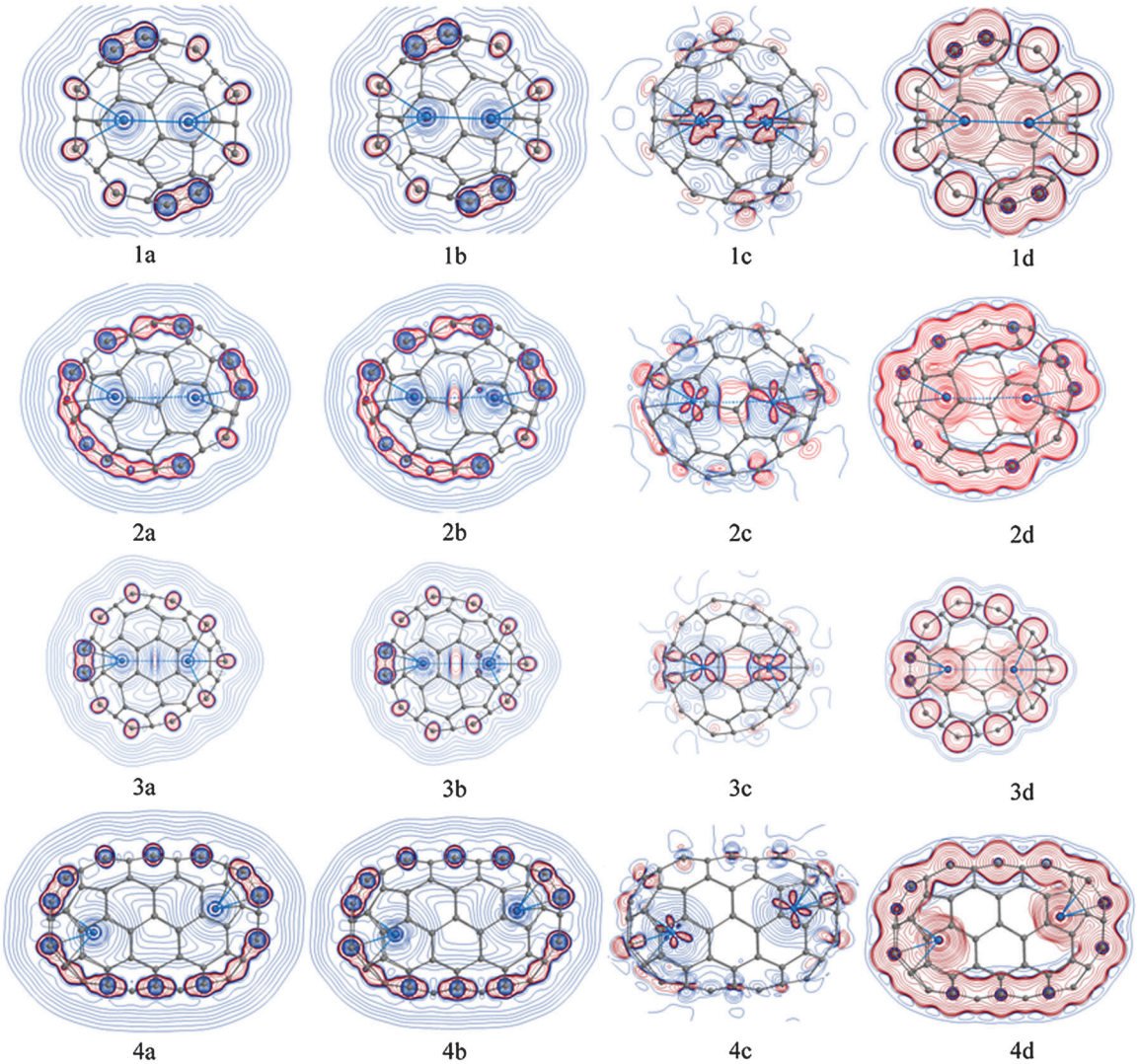

Fig. 6 Profiles of the Laplacian of (a) total electron density, (b) alpha-electron density, (c) spin density, and (d) the energy density for $U_2@C_{60}$ (1), $U_2@C_{70}$ (2), $U_2@C_{84}$ (3), and $U_2@C_{90}$ (4); red and blue lines depict negative and positive regions of each function, respectively.

The delocalization index serves as a seamless quantitative measure of the order of the U–U bond. With a small deviation for $U_2@C_{84}$ the $\delta(U \leftrightarrow U)$ decreases as the U–U distance increases in Table 2. In fact, an exponential correlation can be found with a correlation coefficient of $r^2 = 0.9802$ between r_{U-U} inside a cage and $\delta(U \leftrightarrow U)$, see Fig. 7.

To complete the picture of bonding along the series, we analyzed also the frontier orbitals of the studied compounds, see Fig. S4–S8 in the ESI.† The trends in the MO framework along the series are less straightforward than the results of QTAIM analysis and are only discussed briefly. In accord with the work of Wu and Lu[44] there are six 1e-2c U–U bonding orbitals (one σ-, three π-, and two δ-orbitals) in $U_2@C_{60}$, see Fig. S4 (ESI†). This qualitatively correlates with $\delta(U \leftrightarrow U) = 2.1$. In $U_2@C_{70}$ most of the frontier orbitals are actually bonding but they do not overlap efficiently; only two σ-type orbitals show significant U–U overlap, Fig. S5 (ESI†), which explain lower $\delta(U \leftrightarrow U) = 0.7$ in $U_2@C_{70}$. In $U_2@C_{80}$, we recall the four U–U

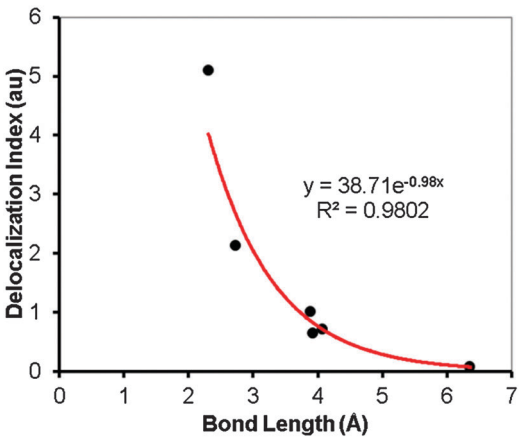

Fig. 7 The plot of $\delta(U \leftrightarrow U)$ *versus* U–U bond length in U_2 (at DI ~ 5) and along the studied $U_2@C_n$ series.

bonding and two U–U antibonding one-electron orbitals (Fig. 2 and Fig. S6, ESI†) and δ(U ↔ U) = 1.0. In $U_2@C_{84}$ there is one σ- and two π-type U–U bonding orbitals (Fig. S7, ESI†) but the latter are only weakly overlapping, which explains lower δ(U ↔ U) of 0.7. No U–U bonding orbitals are observed in $U_2@C_{90}$ (Fig. S8, ESI†). The definition of the bond order using MO analysis is thus not straightforward. The delocalization index appears as a more genuine and general parameter to be used in the present context.

Finally, the U–U bonding inside a fullerene cage can be regarded as an unwilling bonding. The uranium atoms strongly bind to the cage and acquire a positive charge.[53] The calculated NPA charges in Table 2 on uranium atoms vary from 0.1 in $U_2@C_{60}$ and 0.4 in $U_2@C_{70}$ to ∼0.8 in larger fullerenes. To compensate for the U–U charge repulsion, the electron density in U(5f) shells delocalizes between the uranium atoms thus making one-electron-two-center U–U bonds. In a small cage, like $U_2@C_{60}$, covalent multiple U–U bonding with DI(U ↔ U) = 2.1 is forced by the short U–U distance. In larger cages, C_{70} through C_{84}, the U–U bonding of the order of single bond is still predicted, even at $r_{U-U} \sim 4$ Å, with DI(U ↔ U) between 0.7 and 1.0. In $U_2@C_{90}$, strong U–cage interactions and the interior of the cage do not, in principle, prevent U–U bonding but the charge–charge repulsion forces the encapsulated atoms to separate at large distances.

4 Conclusions

In this work, we have theoretically characterized the $U_2@C_{80}$ compound, reported previously in the TOF-MS experiments. We show that it is an endohedral open-shell septet $^7U_2@C_{80}$ system with six unpaired electrons residing mainly in the U(5f) shell. It is derived from the C_{80}:7 fullerene cage. The encapsulated uranium atoms are strongly bound to the cage by polarized covalent bonding, as evidenced by the large encapsulation energy of U_2 in C_{80} and by bonding analysis. MO analysis reveals a double ferromagnetic 1e-2c U–U bond between uranium atoms in the $^7U_2@C_{80}$:7 minimum structure. The U–U bonding is further confirmed by the QTAIM delocalization index, δ(U ↔ U) = 1.01, corresponding to a single bond. This bonding is realized even at a relatively large U–U distance of ∼3.9 Å and arises from U(5f)–U(5f)-based singly occupied MOs. The thermodynamical estimate of the U–U interactions inside $^7U_2@C_{80}$:7 was calculated to be attractive, −17.7 kcal mol^{-1}.

To obtain a more general picture of the endohedral U–U interactions, a series of di-uranium compounds, $U_2@C_n$ (n = 60, 70, 80, 84, 90), was analyzed. A U–U bonding of the order of a single bond was also identified in $U_2@C_{70}$ and $U_2@C_{84}$ with $r_{U-U} \sim 4$ Å. The character of the U–U bonding and bond order correlates with the U–U distance dictated by the cage, and in this sense can be also tuned by the cage used. The U–U endohedral bonding can be termed as unwilling because it arises from the requirement of the system to decrease the charge–charge repulsion between the encapsulated atoms.

This concept can be extended to other endohedral actinide fullerenes. A preliminary study on the di-thorium fullerenes points to the existence of endohedral Th–Th bonding in C_{80} and C_{70} cages. The results will be published elsewhere.

Note added in proof

A new report on experimental preparation of $U_2@C_{80}$ and other di-uranium fullerenes was published recently.[86]

Acknowledgements

We thank anonymous referees for valuable comments. The project was supported by the Czech Science Foundation, Grant. No. 14-03564S. Institutional support was provided by the Czech Academy of Sciences, project RVO-61388963. C.F.-N. thanks financial support from the SoMoPro II program. The research leading to this work has acquired a financial grant from the People Program (Marie Curie action) of the Seventh Framework Program of EU according to the REA Grant Agreement No. 291782. The research is further co-financed by the South-Moravian Region. Part of the work was carried out at CEITEC – the Central European Institute of Technology with the research infrastructure supported by the project CZ.1.05/1.1.00/02.0068 financed by the European Regional Development Fund. The access to computing and storage facilities owned by parties and projects contributing to the National Grid Infrastructure MetaCentrum, and provided under the program "Projects of Large Infrastructure for Research, Development, and Innovations" (LM2010005), and the CERIT-SC computing and storage facilities, provided under the program Center CERIT Scientific Cloud, part of the Operational Program Research and Development for Innovations (CZ.1.05/3.2.00/08.0144), is acknowledged. We thank Jan Horníček for initial calculations of molecular structures.

References

1 A. Rodriguez-Fortea, S. Irle and J. M. Poblet, *Wiley Interdiscip. Rev.: Comput. Mol. Sci.*, 2011, **1**, 350–367.
2 H. L. Cong, B. Yu, T. Akasaka and X. Lu, *Coord. Chem. Rev.*, 2013, **257**, 2880–2898.
3 X. Lu, T. Akasaka and S. Nagase, *Acc. Chem. Res.*, 2013, **46**, 1627–1635.
4 A. A. Popov, S. Yang and L. Dunsch, *Chem. Rev.*, 2013, **113**, 5989–6113.
5 T. Wang and C. Wang, *Acc. Chem. Res.*, 2014, **47**, 450–458.
6 J. Zhang, S. Stevenson and H. C. Dorn, *Acc. Chem. Res.*, 2013, **46**, 1548–1557.
7 D. M. Rivera-Nazario, J. R. Pinzon, S. Stevenson and L. A. Echegoyen, *J. Phys. Org. Chem.*, 2013, **26**, 194–205.
8 M. Garcia-Borras, S. Osuna, J. M. Luis, M. Swart and M. Sola, *Chem. Soc. Rev.*, 2014, **43**, 5089–5105.
9 P. Jin, C. Tang and Z. Chen, *Coord. Chem. Rev.*, 2014, **270**, 89–111.

10 Y. Zhang and A. A. Popov, *Organometallics*, 2014, **33**, 4537–4549.
11 P. W. Dunk, M. Mulet-Gas, Y. Nakanishi, N. K. Kaiser, A. Rodriguez-Fortea, H. Shinohara, J. M. Poblet, A. G. Marshall and H. W. Kroto, *Nat. Commun.*, 2014, **5**, 8.
12 P. Schwerdtfeger, L. N. Wirz and J. Avery, *Wiley Interdiscip. Rev.: Comput. Mol. Sci.*, 2015, **5**, 96–145.
13 J. Zhao, X. Huang, P. Jin and Z. Chen, *Coord. Chem. Rev.*, 2015, **289**, 315–340.
14 T. Guo, M. D. Diener, Y. Chai, M. J. Alford, R. E. Haufler, S. M. McClure, T. Ohno, J. H. Weaver, G. E. Scuseria and R. E. Smalley, *Science*, 1992, **257**, 1661–1664.
15 M. D. Diener, C. A. Smith and D. K. Veirs, *Chem. Mater.*, 1997, **9**, 1773–1777.
16 K. Akiyama, K. Sueki, Y. L. Zhao, H. Haba, K. Tsukada, T. Kodama, K. Kikuchi, T. Ohtsuki, Y. Nagame, H. Nakahara and A. Katada, in *Nanonetwork Materials: Fullerenes, Nanotubes and Related Systems*, ed. S. Saito, T. Ando, Y. Iwasa, K. Kikuchi, M. Kobayashi and Y. Saito, 2001, vol. 590, pp. 437–440.
17 K. Akiyama, Y. L. Zhao, K. Sueki, K. Tsukada, H. Haba, Y. Nagame, T. Kodama, S. Suzuki, T. Ohtsuki, M. Sakaguchi, K. Kikuchi, M. Katada and H. Nakahara, *J. Am. Chem. Soc.*, 2001, **123**, 181–182.
18 K. Akiyama, K. Sueki, K. Tsukada, T. Yaita, Y. Miyake, H. Haba, M. Asai, T. Kodama, K. Kikuchi, T. Ohtsuki, Y. Nagame, M. Katada and H. Nakaharaa, *J. Nucl. Radiochem. Sci.*, 2002, **3**, 151–154.
19 K. Akiyama, K. Sueki, H. Haba, K. Tsukada, M. Asai, T. Yaita, Y. Nagame, K. Kikuchi, M. Katada and H. Nakahara, *J. Radioanal. Nucl. Chem.*, 2003, **255**, 155–158.
20 P. W. Dunk, N. K. Kaiser, M. Mulet-Gas, A. Rodriguez-Fortea, J. M. Poblet, H. Shinohara, C. L. Hendrickson, A. G. Marshall and H. W. Kroto, *J. Am. Chem. Soc.*, 2012, **134**, 9380–9389.
21 P. W. Fowler, S. J. Austin and J. P. B. Sandall, *J. Chem. Soc., Perkin Trans. 2*, 1993, 795–797.
22 J. Aihara and H. Hosoya, *Bull. Chem. Soc. Jpn.*, 1993, **66**, 1955–1958.
23 K. Jackson, E. Kaxiras and M. R. Pederson, *Phys. Rev. B: Condens. Matter Mater. Phys.*, 1993, **48**, 17556–17561.
24 R. M. Pitzer and K. Zhao, *J. Phys. Chem.*, 1996, **100**, 4798–4802.
25 J.-P. Dognon, C. Clavaguera and P. Pyykko, *J. Am. Chem. Soc.*, 2009, **131**, 238–243.
26 M. V. Ryzhkov, A. L. Ivanovskii and B. Delley, *Comput. Theor. Chem.*, 2012, **985**, 46–52.
27 D. Manna and T. K. Ghanty, *J. Phys. Chem. C*, 2012, **116**, 25630–25641.
28 M. V. Ryzhkov and B. Delley, *Comput. Theor. Chem.*, 2013, **1013**, 70–77.
29 D. Manna and T. K. Ghanty, *J. Phys. Chem. C*, 2013, **117**, 17859–17869.
30 D. Manna, A. Sirohiwal and T. K. Ghanty, *J. Phys. Chem. C*, 2014, **118**, 7211–7221.
31 X. Liu, L. Li, B. Liu, D. Wang, Y. Zhao and X. Gao, *J. Phys. Chem. A*, 2012, **116**, 11651–11655.
32 F. A. Cotton, D. O. Marler and W. Schwotzer, *Inorg. Chem.*, 1984, **23**, 4211–4215.
33 L. Gagliardi and B. O. Roos, *Nature*, 2005, **433**, 848–851.
34 L. N. Gorokhov, A. M. Emelyanov and Y. S. Khodeev, *High Temp.*, 1974, **12**, 1156–1158.
35 L. Gagliardi, P. Pyykko and B. O. Roos, *Phys. Chem. Chem. Phys.*, 2005, **7**, 2415–2417.
36 B. O. Roos, P.-A. Malmqvist and L. Gagliardi, *J. Am. Chem. Soc.*, 2006, **128**, 17000–17006.
37 G. Cavigliasso and N. Kaltsoyannis, *Dalton Trans.*, 2006, 5476–5483.
38 G. La Macchia, M. Brynda and L. Gagliardi, *Angew. Chem., Int. Ed.*, 2006, **45**, 6210–6213.
39 B. O. Roos and L. Gagliardi, *Inorg. Chem.*, 2006, **45**, 803–807.
40 G. Cavigliasso and N. Kaltsoyannis, *Inorg. Chem.*, 2006, **45**, 6828–6839.
41 B. O. Roos, A. C. Borin and L. Gagliardi, *Angew. Chem., Int. Ed.*, 2007, **46**, 1469–1472.
42 G. Cavigliasso and N. Kaltsoyannis, *Inorg. Chem.*, 2007, **46**, 3557–3565.
43 D. A. Penchoff and B. E. Bursten, *Inorg. Chim. Acta*, 2015, **424**, 267–273.
44 X. Wu and X. Lu, *J. Am. Chem. Soc.*, 2007, **129**, 2171–2177.
45 I. Infante, L. Gagliardi and G. E. Scuseria, *J. Am. Chem. Soc.*, 2008, **130**, 7459–7465.
46 X. Dai, Y. Meng, M. Xin, F. Wang, D. Fei, M. Jin, Z. Wang and R. Zhang, *Procedia Chem.*, 2012, **7**, 528–533.
47 X. Dai, J. Han, Y. Gao and Z. G. Wang, *ChemPhysChem*, 2014, **15**, 3871–3876.
48 J. Han, X. Dai, Y. Gao, Y. Meng and Z. Wang, *Phys. Chem. Chem. Phys.*, 2014, **16**, 22784–22790.
49 T. Zuo, L. Xu, C. M. Beavers, M. M. Olmstead, W. Fu, D. Crawford, A. L. Balch and H. C. Dorn, *J. Am. Chem. Soc.*, 2008, **130**, 12992–12997.
50 H. Umemoto, K. Ohashi, T. Inoue, N. Fukui, T. Sugai and H. Shinohara, *Chem. Commun.*, 2010, **46**, 5653–5655.
51 T. Yang, X. Zhao and E. Osawa, *Chem. – Eur. J.*, 2011, **17**, 10230–10234.
52 J. Y. Hao, F. Y. Li, H. J. Li, X. Y. Chen, Y. Y. Zhang, Z. F. Chen and C. Hao, *RSC Adv.*, 2015, **5**, 34383–34389.
53 A. A. Popov, S. M. Avdoshenko, A. Martin Pendas and L. Dunsch, *Chem. Commun.*, 2012, **48**, 8031–8050.
54 C. Schäfer, C. Huber and R. Ahlrichs, *J. Chem. Phys.*, 1994, **100**, 5829.
55 X. Cao and M. Dolg, *J. Mol. Struct.*, 2004, **673**, 203–209.
56 M. J. Frisch, G. W. Trucks, H. B. Schlegel, G. E. Scuseria, M. A. Robb, J. R. Cheeseman, G. Scalmani, V. Barone, B. Mennucci, G. A. Petersson, H. Nakatsuji, M. Caricato, X. Li, H. P. Hratchian, A. F. Izmaylov, J. Bloino, G. Zheng, J. L. Sonnenberg, M. Hada, M. Ehara, K. Toyota, R. Fukuda, J. Hasegawa, M. Ishida, T. Nakajima, Y. Honda, O. Kitao, H. Nakai, T. Vreven, J. A. Montgomery, J. E. Peralta, F. Ogliaro, M. Bearpark, J. J. Heyd, E. Brothers, K. N. Kudin, V. N. Staroverov, R. Kobayashi, J. Normand, K. Raghavachari, A. Rendell, J. C. Burant, S. S. Iyengar, J. Tomasi, M. Cossi, N. Rega, J. M. Millam, M. Klene,

J. E. Knox, J. B. Cross, V. Bakken, C. Adamo, J. Jaramillo, R. Gomperts, R. E. Stratmann, O. Yazyev, A. J. Austin, R. Cammi, C. Pomelli, J. W. Ochterski, R. L. Martin, K. Morokuma, V. G. Zakrzewski, G. A. Voth, P. Salvador, J. J. Dannenberg, S. Dapprich, A. D. Daniels, Ö Farkas, J. B. Foresman and J. V. Ortiz, J. Cioslowski, D. J. Fox, *Gaussian 09, Revision D.01*, Wallingford CT, 2009.

57 R. Ahlrichs, M. Bär, M. Häser, H. Horn and C. Kölmel, *Chem. Phys. Lett.*, 1989, **162**, 165–169.

58 A. E. Reed, L. A. Curtiss and F. Weinhold, *Chem. Rev.*, 1988, **88**, 899–926.

59 A. E. Reed, R. B. Weinstock and F. Weinhold, *J. Chem. Phys.*, 1985, **83**, 735–746.

60 T. Lu and F. Chen, *J. Comput. Chem.*, 2012, **33**, 580–592.

61 W. Humphrey, A. Dalke and K. Schulten, *J. Mol. Graphics Modell.*, 1996, **14**, 33–38.

62 M.-L. Sun, Z. Slanina, S.-L. Lee and F. Uhlík, *Chem. Phys. Lett.*, 1995, **246**, 66–72.

63 R. W. F. Bader, *Atoms in Molecules: A Quantum Theory*, Oxford University Press, Oxford, 1990.

64 P. L. A. Popelier, *Atoms in Molecules an Introduction*, Pearson, London, 2000.

65 A. A. Popov and L. Dunsch, *Chem. – Eur. J.*, 2009, **15**, 9707–9729.

66 Z. Badri, C. Foroutan-Nejad and P. Rashidi-Ranjbar, *Comput. Theor. Chem.*, 2013, **1009**, 103–107.

67 Y. Kolokoltsev, D. P. Sanders and V. A. Basiuk, *J. Comput. Theor. Nanosci.*, 2015, **12**, 674–681.

68 C. Foroutan-Nejad, S. Shahbazian and R. Marek, *Chem. – Eur. J.*, 2014, **20**, 10140.

69 D. Cremer and E. Kraka, *Angew. Chem., Int. Ed.*, 1984, **23**, 627–628.

70 M. Rafat and P. L. A. Popelier, in *The quantum theory of atoms in molecules: from solid state to DNA and drug design.*, ed. C. F. Matta and R. J. Boyed, Willey-VCH, Weinheim, 2007, p. 121.

71 M. García-Revilla, E. Francisco, P. L. A. Popelier and A. Martín-Pendás, *ChemPhysChem*, 2013, **14**, 1211–1218.

72 F. Cortés-Guzmán and R. F. W. Bader, *Coord. Chem. Rev.*, 2005, **249**, 633–662.

73 T. A. Keith, *AIMAll, version 13.05.06*, http://aim.tkgristmill.com.

74 T. Yumura, Y. Sato, K. Suenaga and S. Iijima, *J. Phys. Chem. B*, 2005, **109**, 20251–20255.

75 K. Muthukumar and J. A. Larsson, *J. Mater. Chem.*, 2008, **18**, 3347–3351.

76 L. Feng, M. Suzuki, N. Mizorogi, X. Lu, M. Yamada, T. Akasaka and S. Nagase, *Chem. – Eur. J.*, 2013, **19**, 988–993.

77 J. E. Huheey, E. A. Keiter and L. L. Keiter, *Inorganic Chemistry: Principles of Structure and Reactivity, Fourth Edition*, HarperCollins College Publishers, New York, 1993.

78 P. W. Fowler and D. E. Manolopoulos, *An Atlas of Fullerenes*, Oxford University Press, Oxford, U.K., 1995.

79 P. Pyykkö, *J. Phys. Chem. A*, 2015, **119**, 2326–2337.

80 X. Y. Cao, W. J. Liu and M. Dolg, *Sci. China, Ser. B: Chem.*, 2002, **45**, 91–96.

81 X. Y. Cao and M. Dolg, *Theor. Chem. Acc.*, 2002, **108**, 143–149.

82 T. Kato, *J. Mol. Struct.*, 2007, **838**, 84–88.

83 M. Yamada, T. Wakahara, Y. Lian, T. Tsuchiya, T. Akasaka, M. Waelchli, N. Mizorogi, S. Nagase and K. M. Kadish, *J. Am. Chem. Soc.*, 2006, **128**, 1400–1401.

84 S. Taubert, M. Straka, T. O. Pennanen, D. Sundholm and J. Vaara, *Phys. Chem. Chem. Phys.*, 2008, **10**, 7158–7168.

85 Y. Zhang, D. Krylov, M. Rosenkranz, S. Schiemenz and A. A. Popov, *Chem. Sci.*, 2015, **6**, 2328–2341.

86 L. Echegoyen and D. Buck, in *227th ECS Meeting*, Chicago, IL, 2015, abstract 817.